Electron-Cloud Effects in the LHC *

F. Zimmermann, CERN, Geneva, Switzerland

Abstract

We describe the simulated electron-cloud build up inside the vacuum chamber of the Large Hadron Collider (LHC) and its possible impact on the machine performance. The predictions are based on computer simulation programmes which have been calibrated against laboratory measurements of surface properties as well as against observations in existing accelerators (SPS, PS, KEKB). For the LHC, the major concern is the electron heat load inside the cold magnets. Various possible countermeasures are also discussed.

1 INTRODUCTION

There are four electron-cloud effects which could affect the performance of the LHC: (1) the head load deposited on the beam screen in the LHC arcs, (2) the heat load passing through the pumping slots onto the cold bore of the superconducting magnets, (3) the beam instability at injection into the LHC, and (4) the vacuum pressure rise and electron-induced gas desorption in the LHC straight sections. The last aspect is considered in a separate presentation [1] and will not be discussed here. In this report, we will describe the first three, then outline the LHC recipe for combatting the electron cloud, and finally comment on a future luminosity upgrade.

2 ELECTRON BUILD UP

The electron cloud is generated by either of three production mechanisms or a combination thereof.

In the LHC at injection primary electrons are produced by residual gas ionization. The design hydrogen density is 10^{15} molecules/m^3 and the CO density 1.3×10^{14} molecules/m^3 [3]. (For comparison, a pressure of 1 nTorr at 300 K corresponds to 3×10^{13} molecules/m^3). The ionization cross sections for hydrogen and CO molecules are about 0.16 and 1.5 Mbarn, respectively [4]. Then, for a beam current of 0.7 A, the typical production rate of primary electrons due to ionization is of the order $d^2\lambda_e/(ds\ dt) \approx 2 \times 10^{11}$ e$^-$ m^{-1}s^{-1}.

At 7 TeV the largest source of primary electrons is synchrotron radiation and photo-emission. Assuming a bending radius of $\rho \approx 1$ km, $\gamma = 10^6$ and a photoelectron yield $Y^* \approx 0.1$, about one photo-electron is emitted per positron or proton and per meter. For these numbers, and taking a beam current of about 0.7 A, we find an electron production rate of $d^2\lambda_e/(ds\ dt) \approx 5 \times 10^{15}$ e$^-$ m^{-1}s^{-1}, *i.e.*, the number of photoelectrons is 4 orders of magnitude higher than that from ionization.

Finally, the third production mechanism of electrons is secondary emission or beam-induced multipacting. This can lead to an exponential increase in the electron density during the passage of a bunch train. The secondary electrons themselves consist of two components: (1) secondaries, and (2) elastically reflected and rediffused electrons.

The true secondary electrons have an initial energy of a few eV, the elastic electrons an energy equal to the energy of the incident electron, the rediffused an energy somewhere in between. Our latest simulations [6] distinguish between the true and the elastically reflected electrons. Both components are represented based on measurements and parametrizations for LHC vacuum chamber prototypes [5]. For small incident energies (a few eV), the probability of elastic reflection is 30–50%, depending on the surface conditioning.

In simulations of the electron-cloud build up in the LHC [6] the elastic reflection is modelled as follows. Whenever a (macro-)electron hits the wall, we change the charge attributed to that macro-electron according to the total secondary emission yield at this value of incident energy. We then determine randomly whether the secondary (macro-)electron is elastically reflected or a true secondary. If it is elastically reflected, we preserve the absolute momentum of the macro-particle and invert its momentum component normal to the wall.

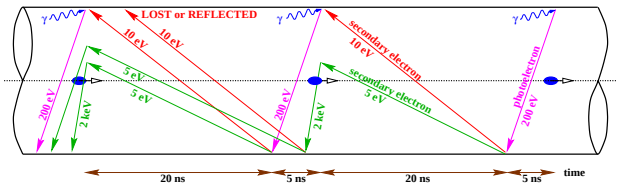

Figure 1: Schematic of electron-cloud build up in the LHC.

Figure 1 illustrates how the number of electrons is amplified during the passage of an LHC bunch train. The LHC bunches are spaced by 25 ns. For nominal bunch current, a photoelectron created on the wall while the head of a bunch is passing is accelerated to about 200 eV by the beam field and reaches the other side of the wall about 5 ns later, well before the next bunch arrives. The electron energy is high enough to produce a significant number of secondaries, which move slowly across the chamber and can be accelerated by the following bunch.

For a bunch current that is about five times lower, the

* LHC electron-cloud studies are performed in collaboration with G. Rumolo, G. Arduini, V. Baglin, S. Berg, O. Bruning, F. Caspers, A. Chao, R. Cimino, I. Collins, K. Cornelis, H. Fukuma, M. Furman, O. Grobner, S. Heifets, N. Hilleret, M. Jimenez, K. Ohmi, E. Perevedentsev, M. Pivi, A. Rossi, F. Ruggiero, G. Stupakov, L. Wang, and many others.

velocity gained by the photoelectrons would also be five times slower, and in this case they would need about 25 ns to traverse the chamber. This corresponds to the so-called multipacting condition [2]

$$n_{\min} \equiv \frac{h_y^2}{N_b r_e L_{\rm sep}} = 1\,, \qquad (1)$$

where h_y denotes the vertical half aperture, $L_{\rm sep}$ the bunch spacing, N_b the bunch population, and r_e the classical electron radius. However, in order to obtain a fast growth rate it is neither sufficient nor necessary to be close to the condition $n_{\min} = 1$, and strong electron-cloud effects are indeed observed for $n_{\min} \gg 1$ as well as for $n_{\min} \ll 1$.

Table 1 lists parameters for the three CERN machines which must accommodate an LHC type beam with 7.48 m bunch spacing. For the LHC two sets of parameters are listed, referring to the initial and final surface conditions, *i.e.*, before and after surface scrubbing due to electron bombardement with a dose larger than 10 mC/mm^2. The measured photoelectron yield per absorbed photon, Y^*, is 10% and 5%, respectively. The photon reflectivity R also diminishes after the scrubbing. The primary electron creation rates per proton and meter, $d\lambda_e/ds$, quoted for SPS and PS correspond to gas ionization with a cross section of 2 Mbarn and to a CO pressure of 50 nTorr and 10 nTorr, respectively. For the two LHC cases the numbers $d\lambda_e/ds$ correspond to a photo-electron yield per adsorbed photon of $Y_e = 0.05$ and $Y_{pe} = 0.025$.

Table 1: Simulation parameters for LHC, SPS, and PS.

symbol	LHC (init.)	LHC (fin.)	SPS	PS
E [GeV]	7000	7000	26	26
N_b	10^{11}	10^{11}	10^{11}	10^{11}
σ_x [mm]	0.3	0.3	3.0	2.4
σ_y [mm]	0.3	0.3	2.3	1.3
σ_z [cm]	7.7	7.7	30	30
$\beta_{x,y}$ [m]	80	80	40	15
L_{sep} [m]	7.48	7.48	7.48	7.48
h_x [mm]	22	22	70	70
h_y [mm]	18	18	22.5	35
$\delta_{\max}$	1.9	1.1	1.9	1.9
$\epsilon_{\max}$ [eV]	262	318	300	300
R [%]	10	5	100	100
$d\lambda_e/ds$ [10^{-6} m^{-1}]	1230	615	0.25	0.05

Figure 2 shows the simulation of electron-cloud build up in an LHC dipole magnet for a maximum secondary emission yield of $\delta_{\max} = 1.5$, and various different bunch populations. For $N_b \geq 4 \times 10^{10}$, the number of electrons increases rapidly.

Figures 3 and 4 illustrate that the energy distribution of electrons incident on the wall and, as a consequence, also the electron-cloud build up strongly depend on the dimension of the vacuum chamber.

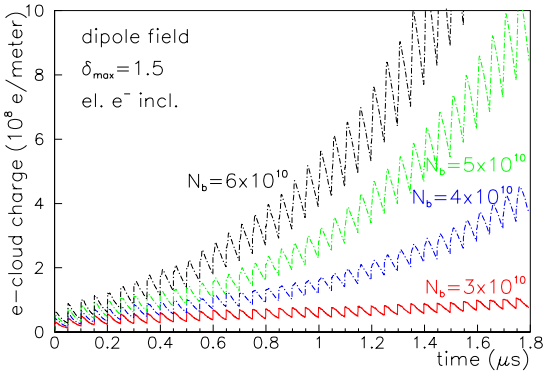

Figure 2: Simulated evolution of electron line density in units of m^{-1} vs. time during the passage of a 72-bunch LHC batch through an LHC dipole chamber for $\delta_{\max} = 1.5$.

The apertures of an SPS dipole magnet, a special SPS calorimeter chamber, and the LHC arcs are compared in Fig. 5. The SPS dipole has almost the same vertical dimension as the beam screen in the LHC arc. Thus in the SPS we can study the electron multipacting under conditions which are close to those expected at the LHC.

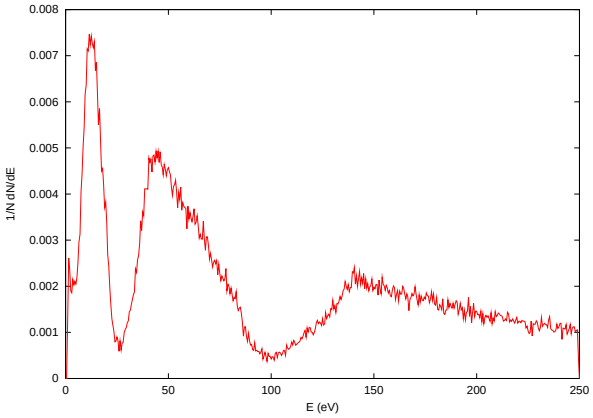

Figure 3: Energy distribution of electrons incident on LHC chamber wall for a round chamber radius $r = 158$ mm.

In Fig. 6 we show the simulated evolution of the electron line density during the passage of three successive LHC bunch trains or "batches" (each batch consists of 72 bunches), considering different batch-to-batch spacings. The electron cloud develops faster for the second and third batch. Thus, gaps larger than 2 μs are required to completely 'reset' the cloud between batches.

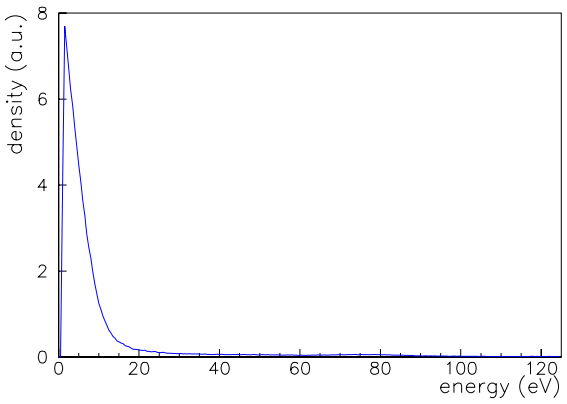

Figure 4: Energy distribution of electrons incident on LHC chamber wall for chamber half dimensions of $h_{x,y} = 22, 18$ mm.

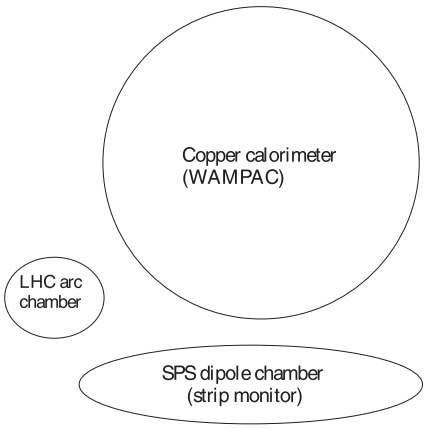

Figure 5: Transverse aperture in the LHC arcs compared with SPS vacuum chambers. Vertical dimension of SPS dipole is similar to LHC arcs.

3 ARC HEAT LOAD

Figure 7 shows the simulated heat load per unit length as a function of bunch population for a quadrupole, a dipole, and a field-free region. The heat load is highest in the field-free region. It is also higher in a quadrupole than in a dipole. This last difference is attributed to the $\cos^2\phi$ distribution of the reflected photons, which is different from earlier simulations where the reflected photons were distributed uniformly around the chamber (according to measurements, the photons are preferentially reflected in the horizontal plane across the chamber, and only few hit the top and bottom; the $\cos^2\phi$ distribution is consistent with data taken in Russia [7]. Different photon distributions were compared in Ref. [8].)

Inclusion of the elastically reflected electrons increases the simulated heat load for the LHC by a factor 2–3 compared with the case where only true secondaries are taken

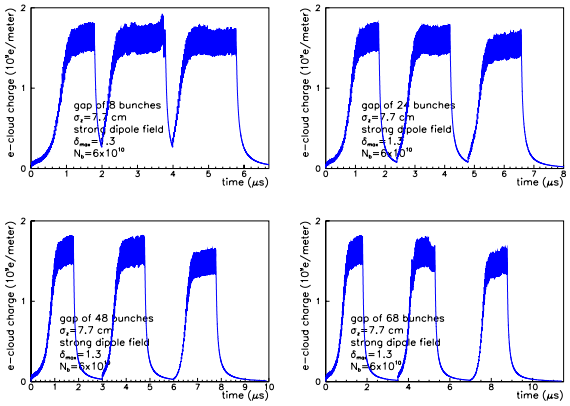

Figure 6: Evolution of electron line density in units of m^{-1} vs. time during the passage of three 72-bunch LHC batches through an LHC dipole chamber, separated by gaps of 8, 24, 48, and 68 missing bunches, for $\delta_{\max} = 1.3$.

into account. The reason why the elastically reflected electrons are so important is that the probability of elastic reflection is highest for low incident energies (for which the true secondary emission yield is small). In the simulation, most of the electrons hitting the beam pipe are yet unperturbed secondaries and have a low energy. The elastic reflection allows them to survive inside the vacuum chamber until the arrival of the next bunch, where they gain additional energy that is deposited on the chamber wall. In other words, the elastic reflection lengthens the survival time of the electrons, and this raises the heat load.

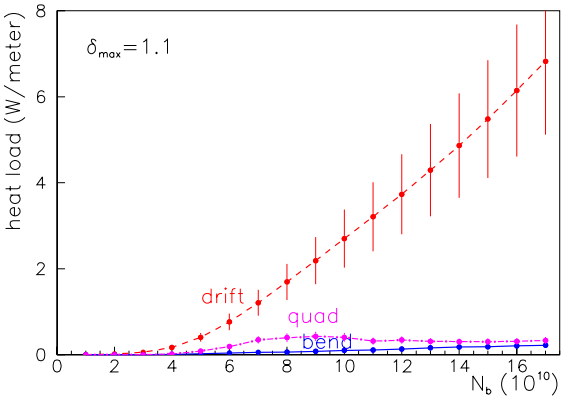

Figure 7: Simulated heat load per unit length in the LHC as a function of bunch population N_b, for various magnetic fields. Other parameters: $\delta_{\max} = 1.1$, $\epsilon_{\max} = 262$ eV, $R = 5\%$, $Y = 5\%$, and elastic electron reflection is included. The dipole field results in the smallest heat load.

Taking into account that each arc half cell comprises $l_{\mathrm{dip}} = 3 \times 14.3$ m $= 42.9$ m of dipole field, $l_{\mathrm{drift}} =$

$(3 \times 1.36 + 2.425)$ m $= 6.505$ m of field-free region, and $l_{\rm quad} = 4.045$ m of quadrupoles, from simulations such as those in Fig. 7 the average heat load per meter in the LHC arcs can be computed. This is shown in Fig. 8 as a function of bunch intensity, together with the available cooling capacity. The cooling capacity decreases for higher currents, since the cooling needs for synchrotron radiation and impedance heating increase linearly and quadratically with current, respectively. For the ultimate intensity of $N_b = 1.67 \times 10^{10}$ the average arc heat load from the chamber impedance is estimated to be about 0.41 W/m and that from synchrotron radiation 0.25 W/m [9].

The different heat-load curves in Fig. 8 refer to different values of $\delta_{\rm max}$. In most cases a steep increase in the heat load around $N_b \approx 6 \times 10^{10}$ can be noted. This steep increase will limit the maximum bunch population during the LHC commissioning, for the nominal bunch spacing of 25 ns. According to these simulations, the design bunch population of $N_b = 1.1 \times 10^{11}$ can be reached for $\delta_{\rm max} \approx 1.1$.

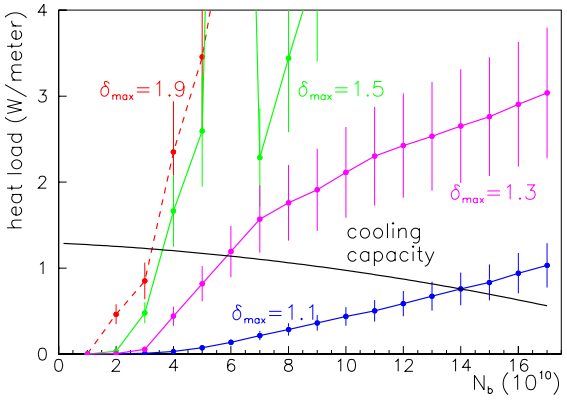

Figure 8: Simulated average LHC arc heat load and cooling capacity as a function of bunch population N_b, for various $\delta_{\rm max}$. Other parameters are $\epsilon_{\rm max} = 262$ eV, $R = 5\%$, $Y = 5\%$, and elastic electron reflection is included.

4 HEAT LOAD ON THE COLD BORE

Figure 9 displays a schematic of the Cu-coated LHC beam screen, which is installed inside the cold bore superconducting magnets and held at a temperature of 5–20 K. The beam screen accommodates several rows of pumping slots, which have a width of 1.5 mm millimeter and a length of 8 mm [10]. The thickness of the beam-screen wall is 1 mm.

Electrons passing through the pumping slots can impinge on the 1.9-K cold bore. The cooling capacity for the cold bore is much smaller than that for the screen, and, hence, an important question is the persistence of multipacting in the presence of the slots and the power deposited through these slots.

In this context, we recall the spatial distibution of electrons multipacting in an LHC dipole field. A typical example is illustrated in Fig. 10. Above about half the nominal bunch population ($N_b \geq 5 \times 10^{10}$), the electron cloud takes the form of two vertical strips with an increased density of electrons. These stripes are attributed to the maximum in the curve of the secondary emission yield as a function of primary electron energy.

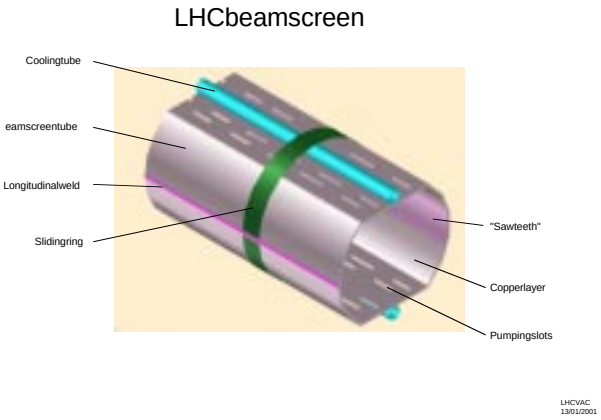

Figure 9: Schematic of the LHC beam screen operating at $T \approx$5–20 K. [Courtesy I. Collins, 2001].

For a reduced bunch population ($N_b < 5 \times 10^{10}$), the cloud concentrates as a single strip around the center of the chamber, since the electrons acquire less energy from a passing bunch.

The horizontal extent of the strips is comparable to the width of the pumping slots. If the strip location coincides with such a slot, a significant portion of the electron cloud could pass through these slots and hit the cold bore.

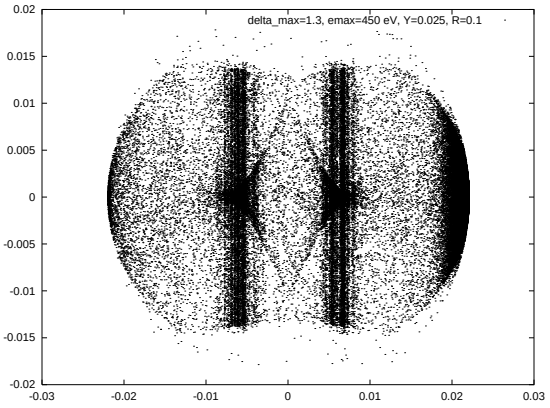

Figure 10: Snapshot of transverse e^- distribution in an LHC dipole chamber, from the first simulation for LHC [11]. Parameters: $\delta_{\rm max} = 1.3$, $\epsilon_{\rm max} = 450$ eV, $R = 0.1$, and $Y^* = 0.025$

The possible suppression of multipacting by the slots is addressed in Figure 11. This figure shows a simulation, performed for a relatively weak dipole field (0.1 T), which explores the effect of many parallel slots, spaced by 5 mm and of varying width (between 0.5 mm and 2 mm), on the

electron-cloud build up. The figure demonstrates that for a transparency as large as 40% (or width 2 mm) the electron impact rate at the position of the slots (treated as perfect absorbers) is not much different from the case without the slots.

This particular simulation was performed for the SPS, in order to predict the performance of the dedicated strip monitor that was subsequently installed, prior to the 2001 SPS run. Given the similarity of the vertical chamber height and the beam parameters, we expect that the situation for the LHC will be about the same.

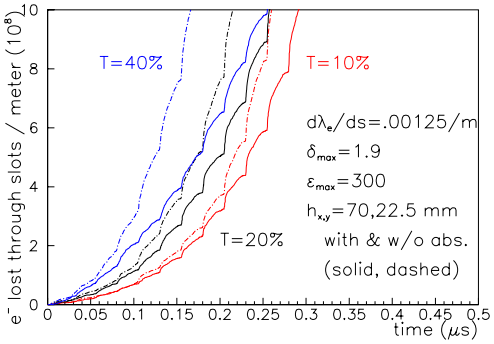

Figure 11: Simulated effect of detector or pumping slot transparency T on electron flow through the slots (solid) compared with the flow in the absence of the slots (dashed). The simulation was performed using a library Runge-Kutta integration, for a field of 0.1 T.

5 INSTABILITIES

The electron cloud can drive both multibunch and single-bunch instabilities. The multi-bunch instability is not believed to be a problem in the LHC [12], due to the high beam energy and the natural betatron frequency spread.

To estimate the strength of the single-bunch instability, we assume that the density of the electron cloud always reaches the neutralization value

$$\rho_{e,\mathrm{sat}} = \frac{N_b}{\pi L_{\mathrm{sep}} h_x h_y} \,, \qquad (2)$$

where N_b is the bunch population, L_{sep} the bunch spacing, $h_{x,y}$ the chamber half dimensions.

Employing a 2-particle model [13] we can estimate the electron density at the TMCI threshold as

$$\rho_{e,\mathrm{thresh}} \approx \frac{2\gamma Q_s}{\pi \beta_y r_p C} \,, \qquad (3)$$

where Q_s denotes the synchrotron tune, β_y the average beta function, r_p the classical proton radius, and C the ring cirumference.

The neutralization and threshold densities for various accelerators at CERN are listed in Table 2. While the PS appears marginally safe, for both the SPS and the LHC the estimated saturation density exceeds the TMCI threshold. In the case of the LHC, the heat load may set a tighter tolerance on the electron density. Nevertheless, Table 2 indicates that the single bunch instability driven by the electron cloud could become a problem at injection into the LHC.

We note that for various machines (KEKB and SPS), the threshold predicted by the 2-particle model was found to be consistent with that obtained from a detailed TMCI calculation using the simulated wake field of the electron cloud [14] and also with the threshold inferred from macroparticle tracking simulations [15, 16].

Table 2 further lists the electron oscillation frequency inside the bunch, $\omega_{e;x,y} \approx c(2N_b r_e/(\sqrt{2\pi}\sigma_z\sigma_{x,y}(\sigma_x + \sigma_y)))^{1/2}$, and the electron density enhancement near the beam axis at the end of the bunch passage H_e ('electron pinch' [17]), which is roughly given by $H_e \approx (1 + 4\sigma_z\omega_{e,x}/(\pi c)) \times (1 + 4\sigma_z\omega_{e,y}/(\pi c))$.

Table 2: Estimated TMCI thresholds for the LHC beam in the PS, SPS, and LHC.

accelerator	PS (26 GeV)	SPS (26 GeV)	LHC (450 GeV)	LHC (7 TeV)
e^- osc./bunch $n_{\mathrm{osc}} \equiv \omega_e\sigma_z/(\pi c)$	1	0.75	0.5	3
density enh. H_e	26	14	8	190
saturation density $\rho_{e,\mathrm{sat}}$ [10^{12} m^{-3}]	1.7	2.7	11.3	11.3
TMCI threshold $\rho_{e,\mathrm{thresh}}$ [10^{12} m^{-3}]	5	0.25	0.56	3
density ratio $\rho_{e,\mathrm{sat}}/\rho_{e,\mathrm{thresh}}$	0.35	11	20	4

6 LHC RECIPE

The present LHC design foresees four measures to suppress the electron cloud:

- In the arc dipoles a sawtooth chamber will be employed in order to reduce the photon reflectivity. Typical longitudinal distance between two sawtooths is 500 μm and their height about 30 μm. Measurement of photon reflectivity and photoemission yields on chamber prototypes were promising [18]. The sawtooth reduces the forward scattered photon reflectivity R to 1.3% (for comparison co-laminated Cu can have $R \approx 80\%$). A prototype sawtooth chamber is shown in Fig. 12.

  Note that although the forward scattered photon reflectivity of the sawtooth is small, the sawtooth may give rise to a 'diffuse' reflection of about 20%. The angular distribution of the diffusely reflected photons is non-uniform; only 10% of these, *i.e.*, 2% of the initial number of photons, will impinge on the bottom

and top of the chamber [19]. In most of the LHC heat-load simulations performed so far, we have assumed a uniform reflectivity R varying between 10% (initial) and 5% (final, *i.e.*, after scrubbing). This resulted in roughly the correct number of photons incident at the top and bottom. Recent simulations consider a $\cos^2\phi$ distribution for the reflected photons, and an associated total reflectivity R of 20%.

- All warm sections in the LHC straights will be coated with the newly developed getter material TiZrV [20], which after activation both provides pumping and lowers the secondary emission yield.

- Surface scrubbing during the commissioning is expected to reduce the maximum secondary emission yield to a low value. Figure 13 shows the decrease of the maximum secondary emission as a function of electron dose, as measured for a copper sample at CERN and SLAC. The CERN data indicate that a value of $\delta_{\max} = 1.1$ is not out of reach. The origin of the discrepancy between the two measurements is unclear.

- As back up solutions, the bunch spacing can be increased or satellite bunches generated to reduce the heat load.

  Figure 14 illustrates that for a 50-ns bunch spacing and a secondary emission yield $\delta_{\max} = 1.3$ (believed to be readily achieved), the bunch population can be raised to the ultimate value of $N_b \approx 1.67 \times 10^{11}$ without exceeding the cooling capacity.

  Figure 15 illustrates the effect of satellite bunches. In this example, we assume that the satellite bunches are created by an incomplete bunch compression in the PS, prior to beam extraction. This results in two satellites spaced by 5 ns, in front and behind the main bunches, respectively. The top picture shows the electron cloud build up for satellites of various intensity, where we keep the total intensity in one main bunch and two satellites constant, equal to 11×10^{10} protons. The bottom picture presents a simulation result for the same values of the main bunch intensity, but without the satellites. We observe that the satellite bunches slow down the blow up, despite of the fact that the total beam current is higher than in the second case.

  The original idea of the satellites was to quickly remove the electrons from the chamber without imparting them enough energy to produce a lot of secondaries [21]. After a significant amount of elastic electron reflection was recently taken into account and included in the simulation, their role was less clear. However, Fig. 15 illustrates that satellite bunches still help, although to a lesser extent than originally anticipated, even if a large part of low-energy electrons are elastically reflected.

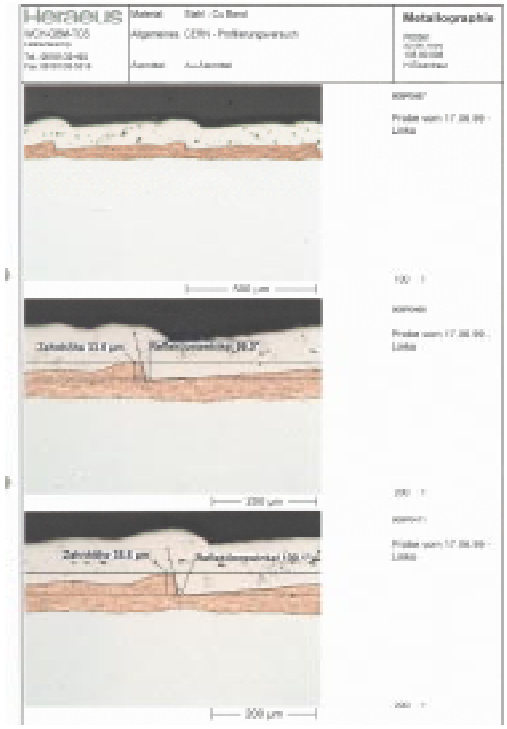

Figure 12: Sawtooth chamber protoype. [Courtesy I. Collins]

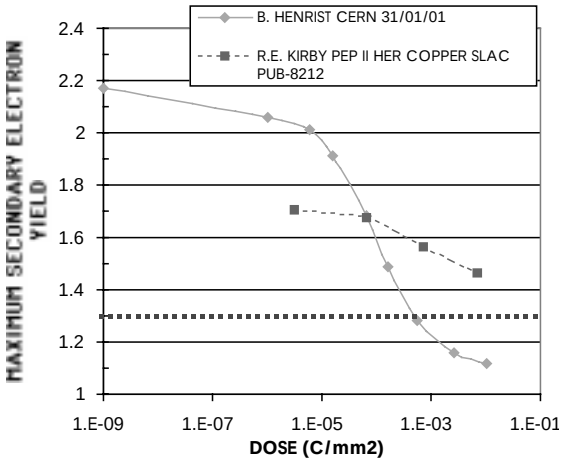

Figure 13: Comparison of dose dependence of the secondary emission yield as measured at CERN and SLAC [5].

7 LHC LUMINOSITY UPGRADE

In the framework of the LHC upgrade study [22], the effect of further shortening the bunch spacing on the arc heat load was also explored by simulation. In Figs. 16 and 17, results are shown for the rather small maximum secondary emission yield of $\delta_{\max} = 1.1$. Even for a value as low as this, the heat load reaches unacceptably high values for the nominal bunch population of $N_b = 1.1 \times 10^{11}$ if the bunch

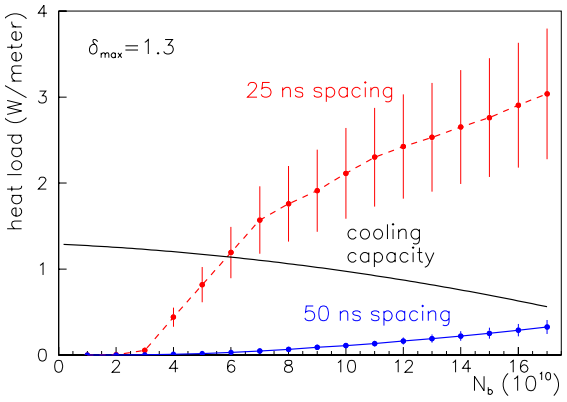

Figure 14: Simulated average LHC arc heat load & cooling capacity as a function of bunch population N_b, for 25 and 50 ns bunch spacing, and $\delta_{\max} = 1.3$. Other parameters are $\epsilon_{\max} = 240$ eV, $R = 5\%$, $Y = 5\%$; elastic electron reflection is included.

spacing is reduced below the canonical value of 25 ns. It is interesting that for higher bunch charges the head load appears to saturate. In Fig. 17 even a small improvement is visible for the shortest spacing of 2.5 ns. We take this as an indication that in the limit of a continuous beam the heat load can be much reduced.

This is further supported by a simulation of the electron-cloud heat load with a long 'superbunch', shown in Fig. 18. For a constant line density, the heat load per passing proton decreases with bunch length. The value of the heat load depends on the longitudinal bunch profile. In this example we considered a flat top with a 10% linearly rising and falling edge.

This result adds a further motivation to the idea of superbunch collisions for a future LHC upgrade. Informations related to the LHC upgrade plans can be found in Refs. [22, 23, 24].

8 CONCLUSIONS

For LHC the most worriesome effects of the electron cloud are the heat load deposited on the beam screen and the electrons passing through the pumping slots. At injection, the single-bunch instability driven by the electrons may also become a problem.

The electron-cloud simulation results are sensitive to certain model parameters, such as $\delta_{\max}$ and the fraction of reflected low-energy electrons.

The simulations predict that the electron cloud is likely to prevent LHC bunch spacings shorter than 25 ns. Superbunch collisions appear to be a promising alternative for future upgrades. They allow further increases in the luminosity while at the same time reducing the electron-cloud heat load.

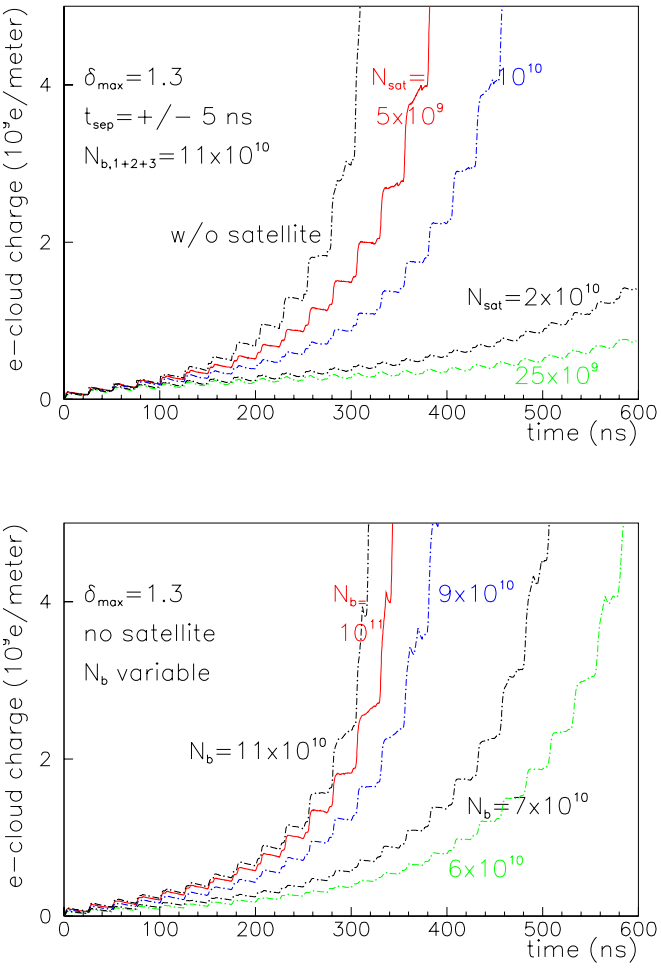

Figure 15: Simulated electron cloud build up in the LHC with (top) and without (bottom) two satellite bunches of various intensity placed one SPS bucket (5 ns) before and after the main bunches. $\sigma_z = 0.3$ m. Elastic e^- reflection included.

9 ACKNOWLEDGEMENTS

I thank G. Rumolo, G. Arduini, V. Baglin, O. Bruning, F. Caspers, A. Chao, R. Cimino, I. Collins, K. Cornelis, H. Fukuma, M. Furman, O. Grobner, S. Heifets, N. Hilleret, M. Jimenez, K. Ohmi, E. Perevedentsev, M. Pivi, A. Rossi, F. Ruggiero, L. Wang, and many others, for helpful discussions, fruitful collaboration, and many useful informations. I am grateful to F. Ruggiero for a careful reading of the manuscript.

10 REFERENCES

[1] A. Rossi, "A Simulation Study of Electron Cloud in the Experimental Regions of the LHC", these proceedings.

[2] O. Gröbner, HEACC'77, Protvino (1977).

[3] N. Hilleret, private communication, February 14, 2002.

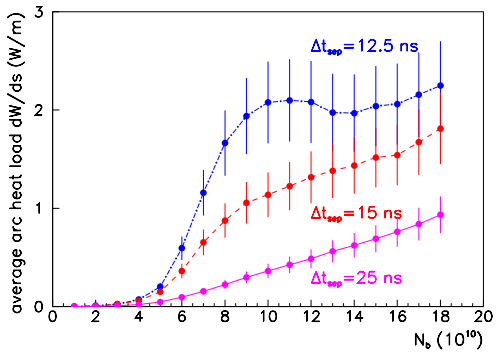

Figure 16: Simulated average arc heat load as a function of bunch population for bunch spacings of 12.5 ns, 15 ns, and 25 ns, and a maximum secondary emission yield $\delta_{\max} = 1.1$. Elastically reflected electrons are included.

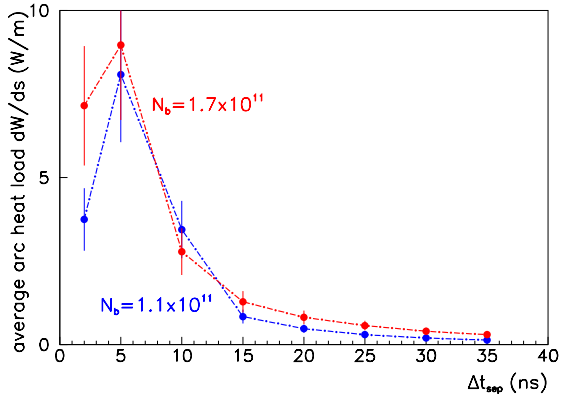

Figure 17: Simulated average arc heat load as a function of bunch spacing, for $\delta_{\max} = 1.1$ and various bunch populations.

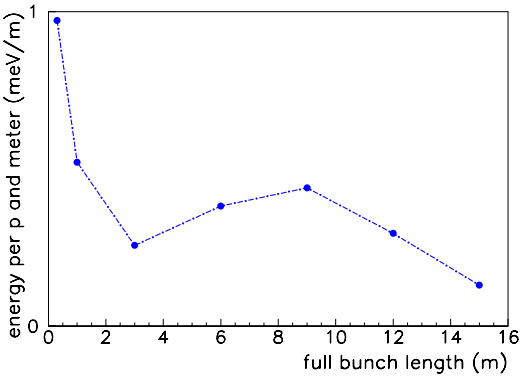

Figure 18: Simulated average energy deposition per proton vs. full bunch length for LHC dipole; line density $\lambda = 10^{12}$ m^{-1} with 10% rising and falling edge.

[4] "Tables and Graphs of Electron-Interaction Cross Sections from 10 eV to 100 GeV Derived from the LLNL Evaluated Electron Data Library (EEDL), Z=1–100", LLNL DE92–007986 (1991).

[5] V. Baglin, I. Collins, B. Henrist, N. Hilleret, G. Vorlaufer, "A Summary of Main Experimental Results Concerning the Secondary Electron Emission of Copper," LHC-Project-Report-472 (2001).

[6] F. Zimmermann, G. Rumolo, "Electron-Cloud Simulations: Build Up and Related Effects," these proceedings (2002).

[7] I. Collins, private communication (2000).

[8] G. Rumolo et al., "Simulation of the Electron-Cloud Build Up and Its Consequences on Heat Load, Beam Stability and Diagnostics," PRST-AB 012801 (2001).

[9] LHC Heat Load Working Group and private communications by L. Evans, L. Tavian and T. Durand (2001).

[10] A. Mostacci, "Beam-Wall Interaction in the LHC Liner," Ph.D. thesis, Universita di Roma 'La Sapienza' (2001).

[11] F. Zimmermann, "A simulation study of electron-cloud instability and beam-induced multipacting in the LHC", LHC Project-Report 95, and SLAC-PUB-7425 (1997).

[12] F. Zimmermann, "Electron-Cloud Simulations for SPS and LHC," Proc. Chamonix X (2000).

[13] K. Ohmi and F. Zimmermann, "Head-Tail Instability Caused by Electron Cloud in Positron Storage Rings", Phys. Rev. Letters 85, p. 3821 (2000).

[14] K. Ohmi, F. Zimmermann, E. Perevedentsev, "Wake Field and Fast Head-Tail Instability caused by an Electron Cloud," Physical Review E 65, 016502 (2002).

[15] G. Rumolo, F. Zimmermann, "Simulation of Single Bunch Instabilities Driven by Electron Cloud in the SPS," Proc. PAC'2001 Chicago, USA, and CERN-SL-2001-041 (AP) (2001).

[16] G. Rumolo, F. Zimmermann, H. Fukuma, K. Ohmi, "Electron Cloud Studies for KEKB," Proc. PAC'2001 Chicago, USA, and CERN-SL-2001-040 (AP) (2001).

[17] M. Furman and A. Zholents, "Incoherent Effects Driven by the Electron Cloud," PAC99, New York (1999).

[18] V. Baglin, I.R. Collins, and O. Grobner, "Photoelectron Yield and Photon Reflectivity from Candidate LHC Vacuum Chamber Materials with Implications to the Vacuum Chamber Design," CERN LHC Project Report 206 (1998), presented at the Sixth European Particle Accelerator Conference (EPAC98), Stockholm (1998).

[19] I. Collins, private communication (2000).

[20] C. Benvenuti, A. Escudeiro Santana and V. Ruzinov, "Ultimate pressures achieved in TiZrV sputter-coated vacuum chambers," Vacuum, Volume 60, Issue 1-2, pp. 279-284 (2001).

[21] F. Ruggiero and X. Zhang, "Collective Instabilities in the LHC: Electron Cloud and Satellite Bunches," in Proc. Workshop on Instabilities of High Intensity Hadron Beams in Rings, BNL, 28 June-1st July 1999, AIP Conf. Proceedings 496, pp. 40-48 (1999).

[22] F. Ruggiero (ed.) et al., "LHC Luminosity and Energy Upgrades: A Feasibility Study," report in preparation.

[23] F. Ruggiero an F. Zimmermann, “Luminosity Optimization Near the Beam-Beam Limit by Increasing Bunch Length or Crossing Angle,” submitted to PRST-AB, CERN-SL-2002-005 (AP) (2002).

[24] K. Takayama, J. Kichiro, M. Sakuda, M. Wake, “Super-bunch Hadron Colliders,” submitted to Physical Review Letters (2001).